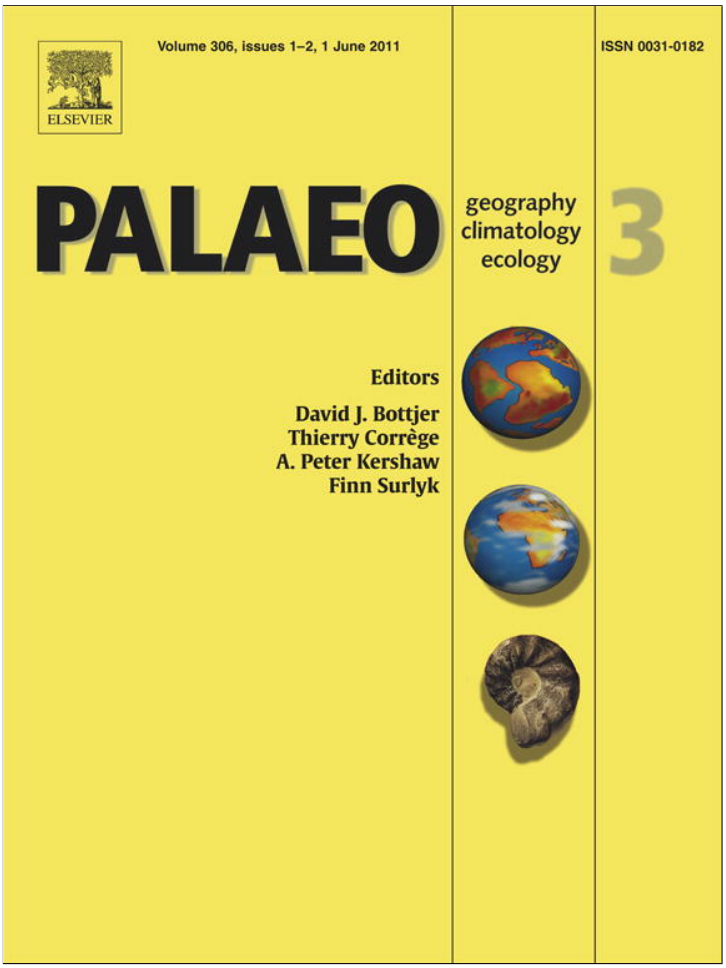

Palaeogeography, Palaeoclimatology, Palaeoecology 306 (2011) 82–94

Contents lists available at ScienceDirect

Palaeogeography, Palaeoclimatology, Palaeoecology

journal homepage: www.elsevier.com/locate/palaeo

On the sensitivity of ocean circulation to arctic freshwater input during the Paleocene/Eocene Thermal Maximum

Jesse T. Cope, Arne Winguth *

University of Texas at Arlington, Arlington, Texas, United States

ARTICLE INFO

Article history:
Received 27 May 2010
Received in revised form 24 March 2011
Accepted 31 March 2011
Available online 12 April 2011

Keywords:
Paleocene/Eocene Thermal Maximum
Carbon isotope excursion
Methane hydrates
Arctic
Ocean circulation
Freshwater
Climate modeling

ABSTRACT

The Paleocene/Eocene Thermal Maximum (PETM) ~55 Ma ago, corresponds to a time characterized by extreme global warming caused by a massive carbon input into the ocean and atmosphere. Climate proxies from sedimentary records suggest that fresh water flow from an ice-free Arctic into the remainder of the global ocean increased due to tectonic changes, enhanced runoff, and thermal expansion. In this study we use the Community Climate System Model version 3 (CCSM-3), including a carbon cycle model, to examine the sensitivity of the ocean circulation to freshwater outflow from the Arctic Ocean during the PETM, and whether these changes may have contributed to an additional warming during the PETM. Two experiments, the first with freshwater exchange between the Arctic and Pacific Oceans and the second between the Arctic and Atlantic Oceans, are compared with a reference experiment with exchange between the Arctic and Indian Oceans and with independent stratigraphic and geochemical records from the Ocean Drilling Program (ODP). As freshwater is transported from the Arctic into the North Pacific Ocean, stratification is enhanced in the North Pacific due to a significant reduction in surface salinity. As a consequence, intermediate to deep-water sources shift from both hemispheres in the Pacific Ocean to a dominant source in the South Pacific Ocean and an additional source in the northern Tethys Ocean. This simulated shift of deep-water sources during the PETM is in agreement with recent Nd isotope measurements. The circulation patterns in the Pacific are similar to those inferred from stable isotope reconstructions, but contradicting a strong North Atlantic deep-water source during the PETM. Freshwater input into the Pacific Ocean results in a warming of intermediate water masses of >2 °C in the North Pacific. When freshwater flow is routed from the Arctic into the Atlantic Ocean, surface density changes are too small to change vertical stratification substantially, contrary to a previous study. In summary, based upon circulation patterns and temperature increases due to freshwater flux through the Bering Strait, Arctic freshwater input into the North Pacific may have contributed to methane hydrate destabilization, an event suggested to have accelerated warming during the PETM.

1. Introduction

The Paleocene Eocene Thermal Maximum (PETM), ~55 Ma ago, was a transient global warming event of a relatively brief duration, characterized by a massive carbon release, and provides an ideal case to study interactions between climate and carbon cycle (e.g., Zachos et al., 2008). Significant changes in the global ocean involved sea surface temperature (SST), deep-sea temperature, calcite compensation depth (CCD), and patterns of global ocean circulation. Sea surface temperatures during this time rose by varying amounts around the globe; the mid-latitude regions were up to 8 °C warmer than background temperatures while the high latitudes were as much as 6 °C warmer (Kelly et al., 2005; Sluijs et al., 2006,2007a; Weijers et al., 2007; Zachos et al., 2003; Zachos et al., 2005). Records from ODP sites indicate deep-sea temperatures 4–5 °C warmer than background (Kennett and Stott, 1991; Thomas and Shackleton, 1996; Tripati and Elderfield, 2005; Zachos et al., 2001) and a CCD, though varying on local levels, that shoaled by up to ~2 km during this time (Kelly et al., 2005; Zachos et al., 2005).

Significant ecological changes occurred during the PETM due to warming and shoreline transgressions (Bowen et al., 2006; Bijl et al., 2009; Sluijs et al., 2007b; Weijers et al., 2007), forcing animals and plants to adapt, migrate and evolve (Woodburne et al., 2009). Examples range from size reduction and dispersion of terrestrial mammals in the northern hemisphere, to range extensions of mid-latitude flora, the increased occurrence of the dinoflagellate cyst Apectodinium (Sluijs et al., 2007a), rapid planktonic foraminifera diversification (Clyde and Gingerich, 1998; Gibbs et al., 2010; Kelly et al., 1998; Wing et al., 2005) and large-scale extinction of benthic foraminifera (Thomas and Shackleton, 1996; Thomas, 1998).

The likely cause of climate change was more than 2000 gigatons of carbon (GtC) entering the atmosphere and ocean over a period of no

* Corresponding author at: Department of Earth and Environmental Sciences, University of Texas at Arlington, 500 Yates St., Arlington, Texas, 76019, United States.
E-mail address: awinguth@uta.edu (A. Winguth).

0031-0182/$ – see front matter © 2011 Elsevier B.V. All rights reserved.
doi:10.1016/j.palaeo.2011.03.032

more than 10,000 years (e.g. Bowen et al., 2004; Zachos et al., 2008). In response to the carbon emissions during the PETM, atmospheric CO_2 levels increased and were in the range of 2000–4000 ppm (Breecker et al., 2010; Zachos et al., 2008) as compared to present levels of ~385 ppm. This carbon release and increase in atmospheric CO_2 concentration is comparable to the amount of carbon to be emitted over the next few centuries due to human activities. Multiple hypotheses have been put forward as the initial trigger of the carbon release. For example, intensive volcanism liberating greenhouse gases could have initiated the warming (Dickens, 2004; Sluijs et al., 2007a; Storey et al., 2007; Svensen et al., 2004). This warming could then lead to a reorganization of the deep sea circulation with bottom water warming, as inferred from isotope ratios (e.g. Dickens et al., 1995; Zachos et al., 2008) and modeling (Bice and Marotzke, 2002; Lunt et al., 2010; Winguth et al., 2010), and could have triggered the injection of carbon through the dissociation of methane hydrates into the climate system.

Topography and bathymetry during the PETM differed significantly from today, with respect to the distribution of landmasses, changes in size of ocean basins and more or less restricted seaways (Fig. 1; Scotese, 2008). Sea levels are affected by tectonic activity (e.g. Larson et al., 2004; Long and Shennan, 1994; Schmitz and Pujalte, 2003; Watts and Thorne, 1984) as well as climatic variability (e.g. Miller et al., 1998; Gale et al., 2002; Antonov et al., 2005; Miller et al., 2005) and are thus difficult to precisely resolve, however, ostracode and dinoflagellate records suggest that sea levels during the PETM rose by approximately 20–30 m from previous levels (Sluijs et al., 2008; Speijer and Morsi, 2002). A connection between the Arctic Ocean and the Tethyan water masses via the Turgay Strait during this time of increased sea level has been inferred from dinoflagellate cysts (e.g. Iakovleva et al., 2001). Limited throughflow via the Fram and Bering Straits due to high sea levels and continued seafloor spreading, is also suggested for the PETM and is supported by Nd–Sr isotopes in fish fossils (Gleason et al., 2009; Roberts et al., 2009) as well as by previous model results and reconstructions (Heinemann et al., 2009; Scotese, 2008). However, the formation of a volcanic bridge between Europe and Greenland (Maclennan and Jones, 2006) would have favored a closed or very narrow and shallow Fram Strait.

Conditions in the Arctic during the PETM are represented by significant increases in sea surface temperature and sea level, and salinity decreases (Sluijs et al., 2006) due to increased runoff from ice melt (Pagani et al., 2006a; Sluijs et al., 2006,2008; Waddell and Moore, 2008) or from enhanced precipitation in high latitudes (Winguth et al., 2010). Fresh water pulses from the Arctic may have affected deep-water formation and the strength of the deep-sea circulation, such as north to south flow in the Atlantic basin. These changes would have influenced global temperature gradients and thus the climate.

The novel approach in this study is to use a fully comprehensive climate model including the marine carbon cycle to explore how changes in the throughflow in ocean passages could have affected the ocean circulation, deep sea temperatures, geochemical tracers and contributed to the global warming during the PETM. For this purpose, sensitivity experiments are carried out comparing a freshwater exchange between the Arctic and the Pacific (Bering Strait) and Atlantic

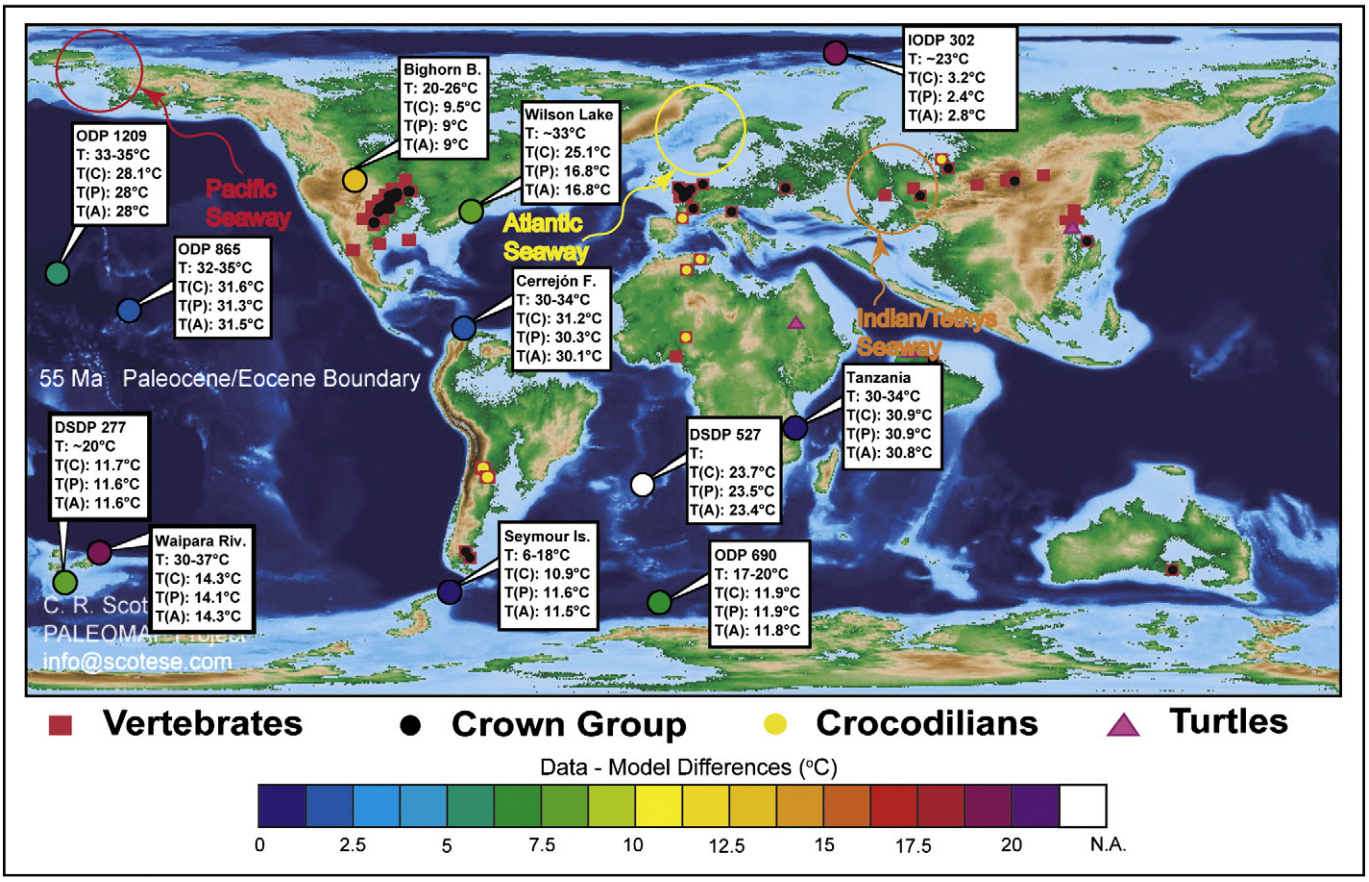

Fig. 1. Geographical reconstruction for the PETM with possible freshwater exchange locations between the Arctic and the remainder of the global ocean; from the PALEOMAP Project (www.scotese.com). The light blue color represents very shallow water (200–500 m), and dark blue are water depths >500 m. Boxes indicate reconstructed surface temperatures across the Paleocene–Eocene boundary for the Control, EOCPAC, and EOCATL experiments (Bralower et al., 2006; Hollis et al., 2009; Ivany et al., 2008; Pearson et al., 2007; Shackleton and Kennett, 1975; Sluijs et al., 2006, 2007b; Sluijs et al., 2008; Thomas et al., 1999; Tripati and Elderfield, 2005; Wing et al., 2005; Zachos et al., 2004; Zachos et al., 2006). Filled circles denote average temperature differences between data and the Control experiment. Fossil locations taken from Markwick (1997). Figure after Winguth et al. (2010).

(Fram Strait) Oceans, respectively. The simulations will be compared with findings Winguth et al. (2010), prescribing the freshwater flux through the Turgay Strait (Arctic-Tethys Seaway), other modeling studies, and climate proxies from the sedimentary record. For example, analysis of Nd isotope data indicates a bimodal ventilation of the deep PETM Pacific with a source of deep water from the North Pacific and even more intense ventilation from the Southern Ocean (Thomas et al., 2003,2008). The analysis of stable carbon isotopes (Nunes and Norris, 2006) from ODP sites indicates an abrupt shift in the deep sea circulation during the PETM with a preference of a northern source, in particular one in the North Atlantic, in agreement with model simulations by Lunt et al. (2010) and Heinemann et al. (2009), but contrary to [CO_3^{2-}] gradients (Zeebe and Zachos, 2007) and model simulations by Winguth et al. (2010).

This paper investigates how Arctic freshwater input into the Pacific Ocean via the Bering Strait or into the Atlantic Ocean via the Fram Strait (for example by sea level rise, by thermal expansion, decrease in basin ocean volume, decrease in mountain glaciers, or local tectonic changes; Harding et al., 2011; Sluijs et al., 2008) would have affected the ocean circulation and distribution of temperature and nutrients during the PETM. The simulations could contribute to a better understanding of the processes leading to methane hydrate destabilization along the slope and rise of continental margins (900–2000 m depth).

2. Model description

2.1. Community Climate System Model 3 (CCSM-3)

The Community Climate System Model 3 (CCSM-3) is a coupled climate model containing four main components: atmosphere, ocean, land, and sea ice, described in detail by Collins et al. (2006). The horizontal resolution is T31×3 in this study.

The coarse resolution of the CCSM-3 T31×3 does not resolve narrow seaways, therefore freshwater flux exchange between the Arctic and the adjacent ocean is parameterized by the marginal sea parameterization (Smith and Gent, 2004). Excess or deficit of freshwater is represented by the transport for each marginal sea *ms* as follows:

$$T_{ms} = \sum_{ms}\left(\left[\max\left(0, QFLUX_{i,j}\right)c_q + \left(E_{i,j} + P_{i,j} + R_{i,j} + M_{i,j}\right) + F^S_{i,j}c_s\right]dx_{i,j}dy_{i,j}\right). \quad (1)$$

Here, T_{ms} is the transport term from the marginal sea (*ms*) in kg s^{-1}, and is dependent on the frazil ice formation (*QFLUX*; in W m^{-2}), evaporation (*E*), precipitation (*P*), river runoff (*R*), and ice melt (*M*) in Kg $m^{-2}s^{-1}$. F^S is the salt flux due to ice melt, and d*x* and d*y* are the zonal and meridional grid spacings in m for grid box with lateral indices *i* and *j*. Conversion factors c_q and c_s are used in order to change units of flux into transport:

$$c_q = -\frac{1}{L_f}\frac{S_o - S_i}{S_o}, c_s = -\frac{1}{S_o}\frac{\rho_{fw}}{\rho_{sw}} \quad (2)$$

where L_f is the latent heat of fusion, S_o is the ocean salinity, S_i is the sea ice salinity, and ρ_{fw} and ρ_{sw} are the densities of freshwater and salt-water respectively (Smith and Gent, 2004). In this approach, direct heat transport from the marginal sea into the adjacent ocean basin can be neglected because feedbacks between temperature and heat fluxes are considered in the marginal sea and because molecular diffusion of heat is ~100× larger than molecular diffusion of salt.

2.2. Ocean carbon cycle model

The marine carbon component of the coupled climate–carbon cycle model is based upon the Ocean Carbon Model Intercomparison Project (OCMIP) (Doney et al., 2006; Najjar and Orr, 1999, http://www.ipsl.jussieu.fr/OCMIP/). The model estimates air–sea fluxes of CO_2 with the wind-dependent gas exchange coefficient (Wanninkhof, 1992) across the air–sea interface, the temperature-dependent solubility of CO_2, and the difference between the prescribed pCO_2 of the atmosphere and the pCO_2 of the uppermost layer of the ocean (Doney et al., 2006). The parameterization of biological uptake of nutrients is similar to that used in the Hamburg Model of the Ocean Carbon Cycle (HAMOCC; Maier-Reimer, 1993) and assumes a constant Redfield ratio for particulate organic matter (POM). The uptake of PO_4 is given by the turnover of biomass, modulated by surface solar irradiance, temperature, and macro- and micronutrients. The carbon cycle model uses a single Martin power-law curve to describe the vertical particulate organic phosphorus flux profile over the full water column. In the deep sea, $\delta^{13}C$ is in first order inversely correlated with the concentration of phosphate [PO_4] and can be approximated, under the assumption of the present-day isotopic signature of POM and a constant air-sea gas exchange effect, after Broecker and Maier-Reimer (1992) by the following expression:

$$\delta^{13}C = 2.9–1.1[PO_4]. \quad (3)$$

2.3. Topography and land–sea distribution

The land vegetation used in these experiments is modified from that of Sewall et al. (2000), Shellito and Sloan (2006) and Shellito et al. (2003), and is described in Winguth et al. (2010). The twelve vegetation categories or types are those of Dorman and Sellers (1989). The Arctic Ocean is closed because seaways are not resolved by the coarse model resolution and the marginal sea parameteriztion is applied (Section 2.1).

2.4. Radiative forcing

The solar constant for the Paleocene/Eocene boundary is 1362 W m^{-2}, 0.44% lower than the modern value. This value is based upon the curve fit to model results of Boothroyd (Caldeira and Kasting, 1992; Winguth et al., 2002):

$$S(t) = (1-0.38t/t_0)^{-1}S_0. \quad (4)$$

$S(t)$ is the luminosity of the Sun at time t, years before present, $t_0$is 4.55 Gyr, and $S_0$is the present-day value of luminosity (1368 W m^{-2}). Eccentricity and a moving vernal equinox are set equal to zero, so that the Earth's orbit around the sun is circular and the position of the Earth in its orbit does not change with each year. The use of this circular orbit ensures equal receipt of solar insolation for both hemispheres (Gibbs et al., 2002; Winguth et al., 2002). Earth's obliquity (axis tilt) is set to 23.5°, the same as the modern value.

Atmospheric partial pressure of CO_2 (pCO_2) is set to 2240 ppm for the PETM, about 8× pre-industrial level (Winguth et al., 2010). This level agrees with Breecker et al., (2010), and Zachos et al. (2008), but is low according to estimates from Hsieh and Yapp (1999), Pearson and Palmer (2000), and Zachos et al. (2001). Pagani et al. (2006b) suggest that levels of CO_2 could have been much higher if viewed as the only forcing mechanism for climate change. N_2O levels were set at 0.275 ppb and CH_4 levels at 0.700 ppb, both representative of pre-industrial values. The CH_4 level is not changed from its pre-industrial value because the residence time for CH_4 in the atmosphere is less than ten years, and it oxidizes to CO_2 (Wallace and Hobbs, 2006).

3. Experimental design and climate simulations

3.1. Initialization conditions of PETM climate simulations

In order to explore the impact of fresh water pulses from the Arctic on the climate and ocean circulation, and the carbon cycle's response

Table 1
Paleolocation and number of model years integrated for each experiment. The marginal sea parameterization is used to model freshwater exchange between the Arctic and global oceans.

Experiment name	Freshwater exchange	Paleolatitude	Paleolongitude	Years integrated
Control	Arctic → Indian/Tethys	40°N	55°	2000
EOCPAC	Arctic → Pacific	60°N	180°	2000
EOCATL	Arctic → Atlantic	50°N	355°	2000

to these changes, two simulations are performed and compared with the 8×CO_2 PETM experiment by Winguth et al., 2010 (referred to hereafter as Control experiment). Exchange between the Arctic and Indian Oceans via the Turgay Street (as in the Control experiment) is based upon the paleogeographic reconstruction with the PALEOMAP Project (Scotese, 2008) as well as data, specifically microfossil data from the Turgay Strait region, from Iakovleva and Heilmann-Clausen (2007), Iakovleva et al. (2001), and Meulenkamp et al. (2000).

The two sensitivity experiments described here are termed EOCPAC and EOCATL. In the EOCPAC experiment freshwater is exchanged between the Arctic and the Pacific whereas in the EOCATL experiment it is exchanged between the Arctic and the Atlantic. The locations of possible Arctic shallow seaways are summarized in Table 1 and shown in Fig. 1. As discussed in Section 1, a flow through the Fram Strait or Bering Strait may have occurred during the PETM either by local tectonic changes, volcanism near Iceland, or sea level rise or a combination of these. All model simulations are integrated over 2000 years with initial conditions as described in Winguth et al. (2010).

3.2. Sensitivity to arctic freshwater pulses in the Pacific (EOCPAC experiment)

3.2.1. Surface stratification and sea level pressure

With the change of fresh water exchange from the Turgay Strait to the Bering Strait, surface salinity levels decrease by ~3 psu to in the North Pacific and increase by ~9 psu in the northern Tethys Ocean

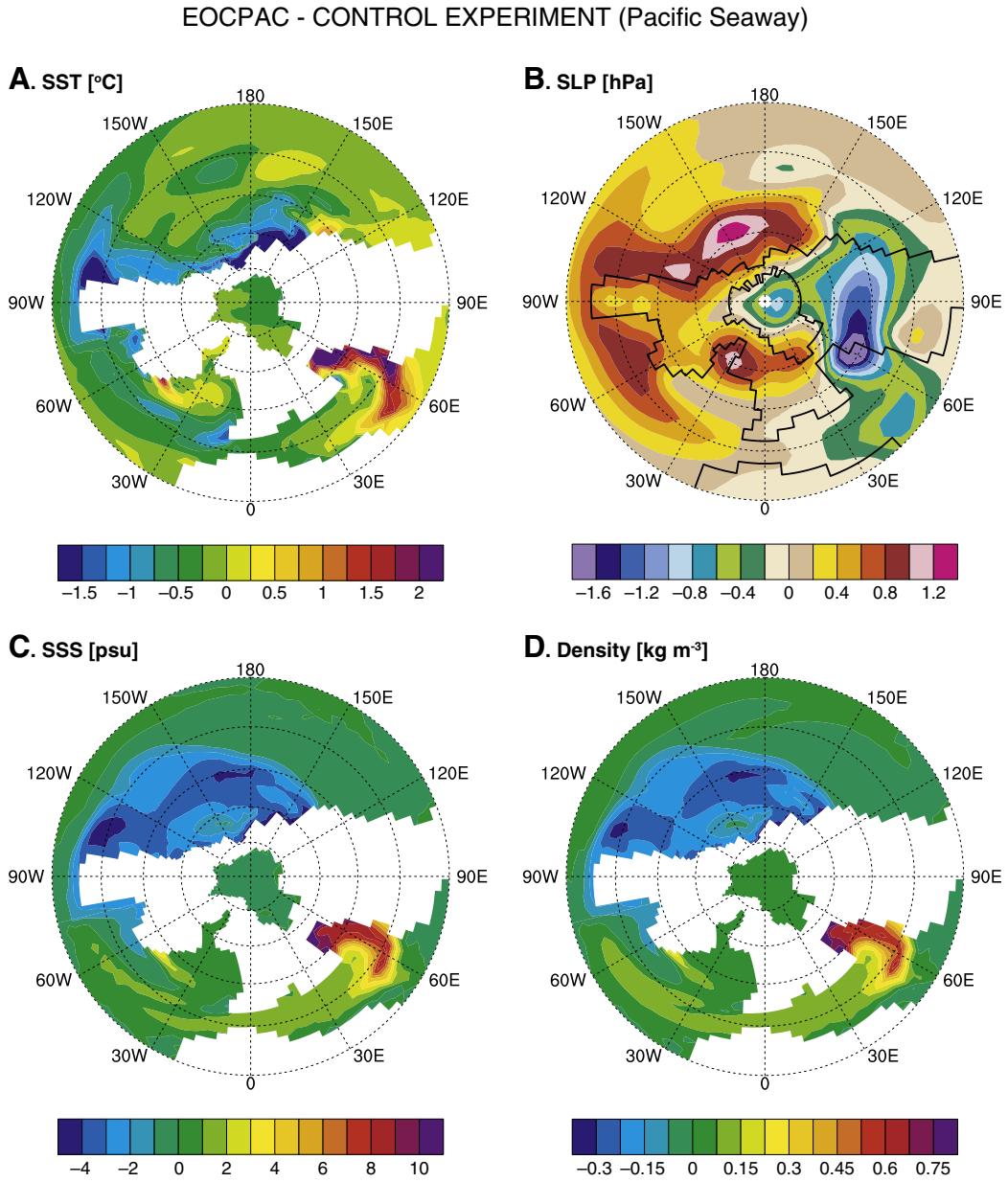

Fig. 2. Northern hemisphere polar projection from 15°N to 90°N, EOCPAC — Control, annual average for years 1950–2000; A) Sea surface temperature (°C), B) surface level pressure (hPa), C) surface salinity (psu), D) surface density.

(Fig. 2). Surface water masses in the North Pacific become more stratified with a decrease in surface salinity and thus surface density.

Changes in sea surface temperature reflect changes in stratification and ocean circulation. Annually averaged sea surface temperatures in the North Pacific poleward of 45°N are around 10–11 °C, a decrease of ~1–2 °C relative to the Control experiment (Fig. 2). Surface temperatures throughout the northern Indian Ocean increase by ~2 °C and by around 1–1.5 °C off the east coast of North America, compared to the Control experiment. The east–west temperature gradient across the Pacific is about ~1.5–2 °C stronger than in the Control experiment.

Sea level pressure differences between the sensitivity experiments are most pronounced over the northern hemisphere (Fig. 2). Off the North American west coast, differences in sea level pressure of +1 hPa between the EOCPAC and Control experiments correlate negatively to sea surface temperatures of ~−1 °C (Fig. 2). Pressure increases in the EOCPAC experiment by ~1–1.5 hPa over the North Pacific compared to the Control experiment. It decreases over the northern Indian Ocean and southwestern Asia by ~1.6 hPa.

3.2.2. Mixed layer depth and sources of deep water formation

Relative to the Control experiment, mixed layer depth in the EOCPAC experiment is increased in the northern Tethys and South Pacific, and reduced in the North Pacific and Gulf of Mexico (Fig. 3). In the northern North Pacific, lower salinities and reduced density and mixed layer depth reduces the North Pacific source, whereas in northern Tethys high surface salinity and density increase the mixed layer depth significantly. For both of these locations it appears that the change in location of freshwater input plays a predominant role in deep-water formation. In the South Pacific, temperature is lower, salinity higher, and density higher for the Control experiment. Despite this, the maximum mixed layer depth is deeper and the age of the water mass younger in the EOCPAC experiment, suggesting that the weakening of deep-water formation in the North Pacific results in the strengthening of the deep-water source in the South Pacific. The decline of the northern Pacific source allows warm subtropical water masses to spread further northward leading to a warming of >2 °C in intermediate water depth (Fig. 4).

Compared to the Control experiment, subtropical salinity in the eastern North Atlantic Ocean is reduced by 2 psu (Fig. 2) in the EOCPAC experiment, leading to a reduced mixed-layer depth in the Gulf of Mexico. The resulting buoyancy forcing yields a decrease in maximum mixed layer depth and density and thus a decrease in formation of warm salty intermediate water masses as well as a decrease in temperature in intermediate depth by ~0.6 °C (Figs. 3 and 4).

3.2.3. Meridional Overturning Circulation (MOC)

The global MOC is dominated by the ocean circulation in the Pacific Ocean because the deep sea circulation in the Atlantic is relatively stagnant. The global MOC in Fig. 5 shows a dominant southern source of deep water for the EOCPAC experiment whereas for the Control experiment, deep water sources in both hemispheres are simulated. When comparing the MOC for the Pacific basin only, the EOCPAC

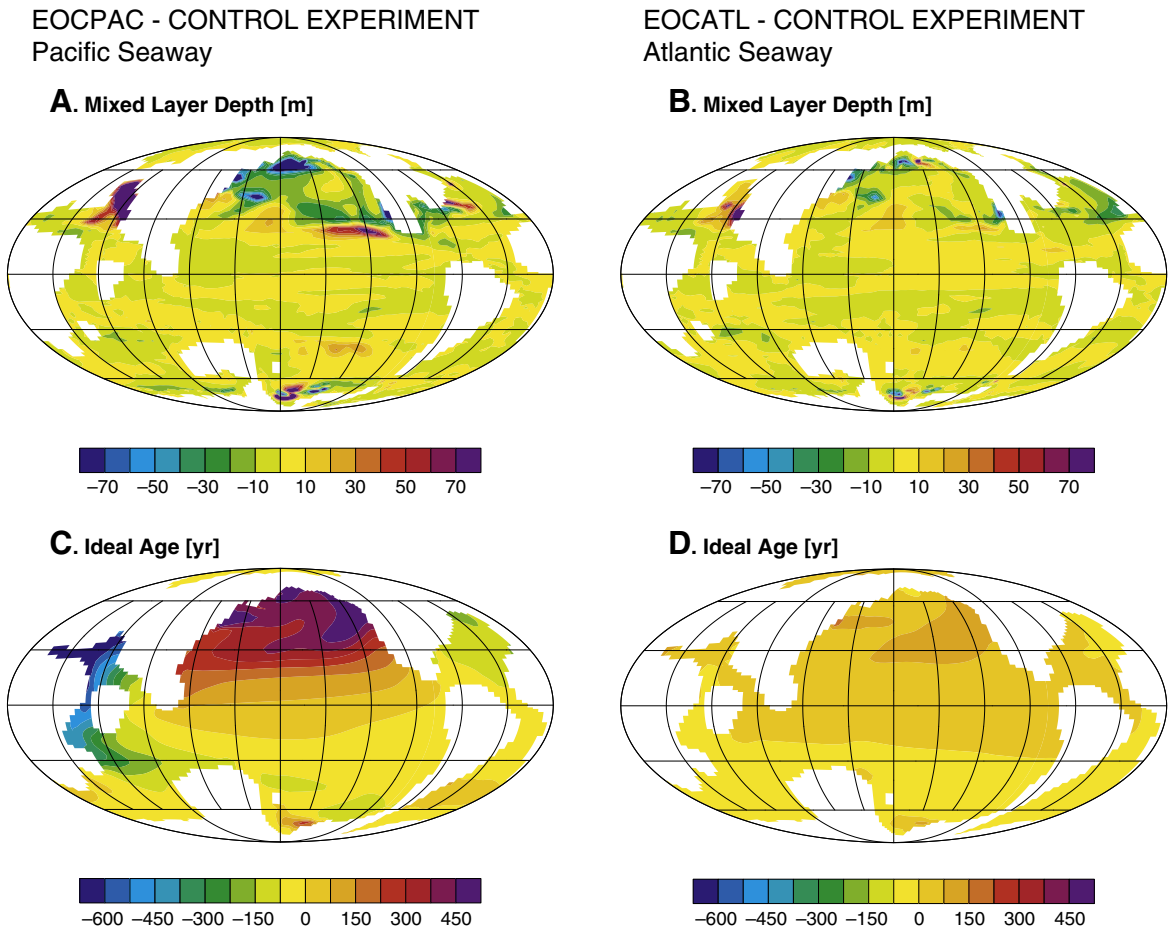

Fig. 3. Projection centered on 180°, annual average years 1950–2000; A) EOCPAC — Control experiment, Maximum Mixed Layer Depth (m), B) EOCATL — Control experiment, Maximum Mixed Layer Depth (m), C) EOCPAC — Control experiment, idealized age (years) in ~1200 m, D) EOCATL — Control experiment, idealized age (years) in ~1200 m. Note that a negative difference in the age means that the ocean circulation is increased in the EOCATL or EOCPAC experiment relative to the control experiment, whereas positive means a reduced circulation.

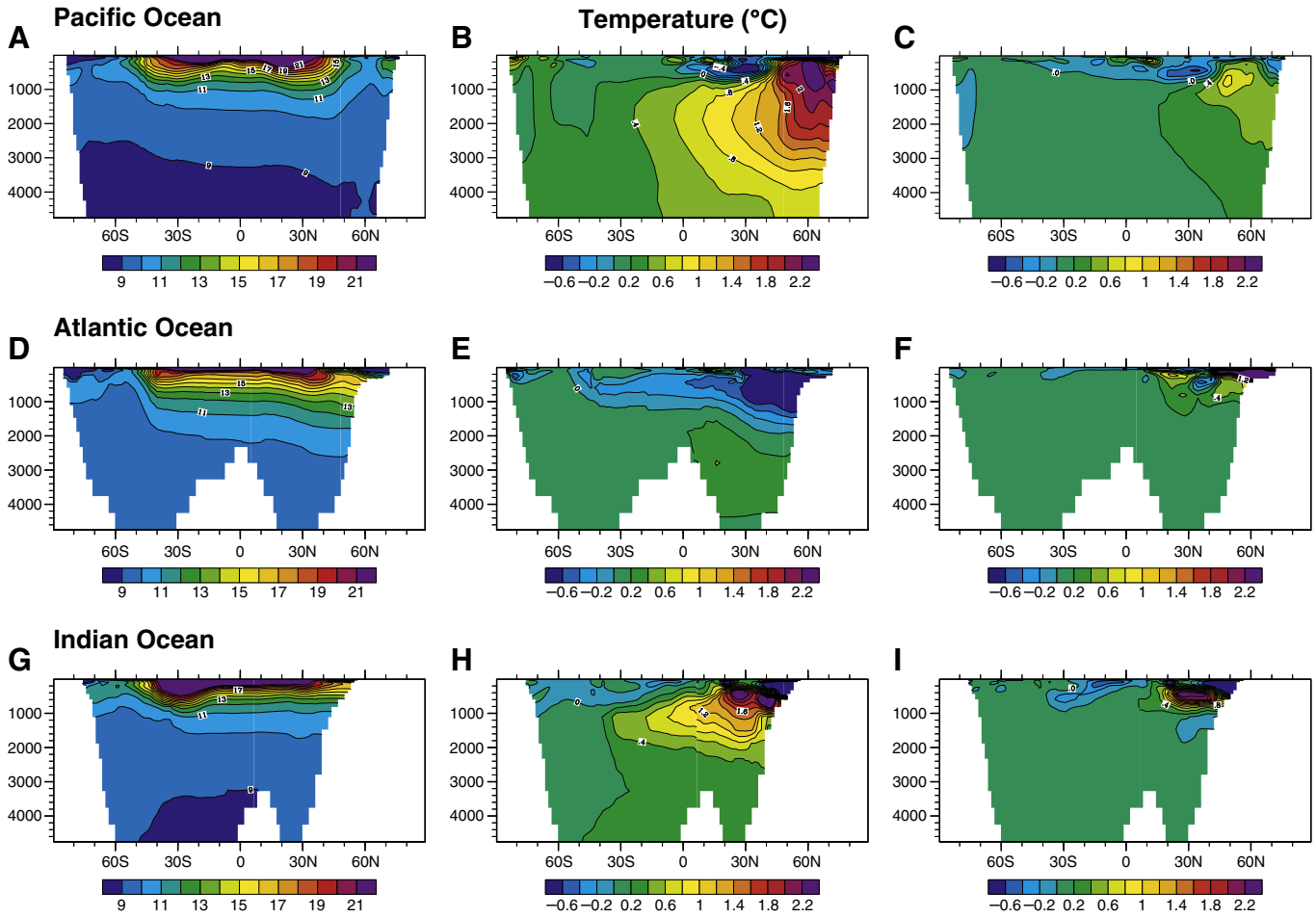

Fig. 4. Vertical sections of potential temperature (50-year mean for the period 1950–2000); Pacific Ocean: A) 8×CO_2 PETM Control experiment, B) differences between the EOCPAC and Control experiments, C) differences between the EOCATL and Control experiments; Atlantic Ocean: D) Control experiment E) differences between the EOCPAC and Control experiments, F) differences between the EOCATL and Control experiments; Indian Ocean: G) Control experiment, H) differences between the EOCPAC and Control experiments, I) differences between the EOCATL and Control experiments.

experiment simulates stronger southward overturning circulation throughout intermediate waters and weaker northward circulation in shallow waters. For the Atlantic basin the EOCPAC experiment demonstrates stronger northward circulation in depths less than 500 m and weaker southward circulation (2 Sv) at intermediate depths north of 40°S.

The increase in southward ocean circulation in the Pacific basin correlates well with the increase in Arctic freshwater flux entering the North Pacific and a reduction in deep-water formation there. In the Atlantic basin, decreased southward flow in the EOCPAC experiment in intermediate waters is correlated with a ~100 year younger water mass and increased northward circulation in shallow depths compared to the Control experiment. In the Indian Ocean basin, increased southward circulation coincides with a younger water mass, deep-water formation in the northern Tethys, and decreased Arctic freshwater flux.

3.2.4. Water masses at intermediate depth

Remarkable differences between the EOPAC and the Control experiment occur throughout intermediate waters (500–1500 m). At ~1200 m, the temperatures in the EOCPAC experiment range from ~9 °C in the South Pacific Ocean, ~11 °C in the northern Tethys Ocean, to ~13 °C in the North Pacific Ocean. Temperatures in the EOCPAC experiment increase in the northwestern Pacific (~2 °C), South Pacific (~0.1 °C), and North Tethys Oceans (~1.5 °C) relative to the Control experiment. Source water mass winter temperatures are 11 ± 3 °C in the northeastern Tethys, 10 ± 2 °C in the Southern Ocean near the east coast of Australia and 13 ± 3 °C in the eastern North Pacific. Compared to the Control experiment, temperatures in the North Atlantic are around 1 °C cooler (Fig. 4).

Ideal age tracers (Fig. 3), a measure of the age of water masses, and the MOC (Fig. 5), highlight a change of sources of intermediate to deep-water masses. In the EOPAC experiment, warm saline water masses are formed in the northeastern Tethys and flowing as an intermediate western boundary current between the African continent and Madagascar into the Southern Ocean where they are mixed with the South Pacific source water, with the youngest water masses (~140 years) near the eastern coast of Australia. The addition of freshwater into the North Pacific changes the strength and origin of intermediate water mass formation throughout the global oceans. Warm saline waters flow into the North Pacific from the western equatorial Pacific due to a reduction in deep water formation there (Figs. 3–5).

At 1200 m, salinity increases in the EOCPAC experiment in the North Pacific near 30°N by ~0.5 psu. At the same depth, a weak increase in salinity is modeled in the northern Tethys Ocean. These changes in salinity are due to a reduction in deep-water formation, advection of warm saline waters from the western Pacific Ocean into the North Pacific, and an increase in deep-water formation and circulation in the northern Indian Ocean, mixing down higher salinity concentrations from the surface.

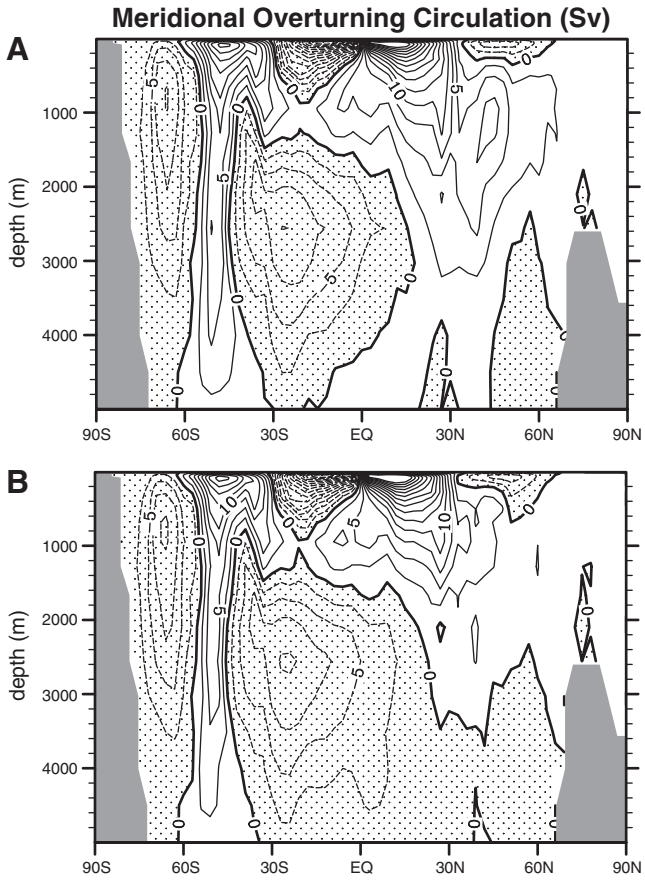

Fig. 5. Annual average of the Eulerian meridional overturning circulation (MOC) in Sv ($1\ Sv = 10^6\ m^3\ s^{-1}$) for years 1950–2000; Global MOC for the A) Control and B) EOCPAC experiments. Flow along positive stream lines is clockwise whereas flow along negative streamlines (dotted area) is anticlockwise.

3.3. Sensitivity to Arctic freshwater pulses in the Atlantic (EOCATL)

3.3.1. Surface stratification and sea level pressure

The EOCATL experiment considers an alternative freshwater exchange between the Arctic and the Atlantic Oceans through the Fram Strait (Table 1 and Fig. 1) instead of the Arctic-Tethys Ocean exchange via the Turgay Strait. Differences in sea surface temperature between the EOCATL and the Control experiments in the North Atlantic and Tethys Oceans correlate well with variations in the location of freshwater flux between the two experiments.

The most pronounced positive differences in sea level pressure occur over the eastern North Pacific Ocean (~1.3 hPa) and over the eastern part of the Atlantic Ocean (~1 hPa; Fig. 6), whereas over the western Pacific Ocean near 60°N and in the northern Tethys Ocean sea level pressure in the EOCATL experiment is reduced by ~0.5 hPa.

In the eastern Atlantic Ocean and North Tethys Oceans sea level pressure correlates negatively to surface atmosphere and ocean temperatures. A significant anomaly (an increase >1.2 hPa) in sea level pressure over the eastern Pacific Ocean is not directly correlated to the sea surface temperature (Fig. 6) and can be linked to changes in the moisture content of the air masses.

Relative to the Control experiment, surface salinity is decreased by ~3–4 psu in the North Atlantic and increased by ~7 psu in the North Indian Ocean (Fig. 6).

3.3.2. Mixed layer depth and sources of deep water formation

Differences between the EOCATL and Control experiments are nominal in most cases, and specific locations tend to show varying trends when comparing temperature, salinity, density, and the maximum mixed layer depth (Fig. 3). Warmer, less dense waters, and a shallower maximum mixed layer depth are simulated for the North Pacific and North Atlantic Oceans. Reduced deep-water formation in the North Pacific and resulting reduced overturning circulation allow for an increase in deep-water formation in the South Pacific and increased northward circulation.

In the South Pacific and northern Tethys, a deeper mixed layer depth in the EOCATL experiment results in cooling compared to the Control experiment. Both locations depict decreased salinity despite deeper mixed layer depths. Density is greater in the EOCATL experiment in the northern Tethys due to saline deep-water formation, but lower than the density of the underlying water masses from the central Pacific.

3.3.3. Meridional Overturning Circulation (MOC)

The overturning circulation in the EOCATL experiment is similar to the Control experiment, showing only small changes of <2 Sv in both the shallow and deep ocean with a weakened North Pacific source.

3.3.4. Water masses of intermediate depth

As discussed in Section 3.3.2, the mixed layer depth is stronger in the northern Tethys, North Atlantic, and South Pacific Oceans, and weaker in the North Pacific Ocean for the EOCATL experiment compared to the Control experiment. For the North Pacific Ocean temperatures in the EOCATL experiment increase by up to 1 °C and the idealized age is ~140–150 years older compared to the Control experiment (Figs. 3 and 4) in response to a weaker polar source.

4. Discussion

Ocean deep-water formation is sensitive to changes in surface buoyancy and momentum fluxes. In the EOCPAC experiment, salinity increase by increased freshwater input via the Bering Strait enhances the stratification in the North Pacific Ocean relative to the Control experiment and weakens the North Pacific source of intermediate water. The intermediate water masses in this region are predominantly controlled by a subtropical source resulting in an increase in ideal age of these water masses. In the northern Tethys, the mixed layer depth in the EOCPAC experiment is significantly deepened due to an increase in salinity, producing warm and saline intermediate water that flows as a western boundary current into the Southern Ocean.

In the EOCATL experiment, a freshwater exchange from the Arctic to the Atlantic Ocean via the Fram Strait does not influence the properties of intermediate water masses in the Atlantic or Indian Ocean substantially, but the North Pacific intermediate water masses increase in temperature and ideal age in response to a weaker Northern Pacific source.

Potential temperatures of intermediate waters are higher throughout most of the global ocean and specifically in the Pacific basin in the EOCPAC experiment compared to the Control experiment. Increased temperatures in intermediate waters in the EOCPAC experiment suggest that an increase in freshwater input into the North Pacific through the Bering Strait during the late Paleocene might have led to increased warming across the globe which in turn could have triggered the release of methane hydrates (e.g. Sluijs et al., 2007a; Thomas et al., 2002). This methane release might therefore have contributed to a temperature increase during the PETM.

In the EOCPAC experiment, increased temperatures in the western Pacific and North Atlantic Oceans near 45°N coincide with increased freshwater input into the North Pacific Ocean (Figs. 1 and 2), whereas with increased freshwater input into the North Atlantic Ocean in the EOCATL experiment, surface temperatures decrease in the subtropical North Pacific. The changes in freshwater input into the North Pacific and the associated warming of intermediate water masses also affect other oceans, for example the intermediate water formation in the

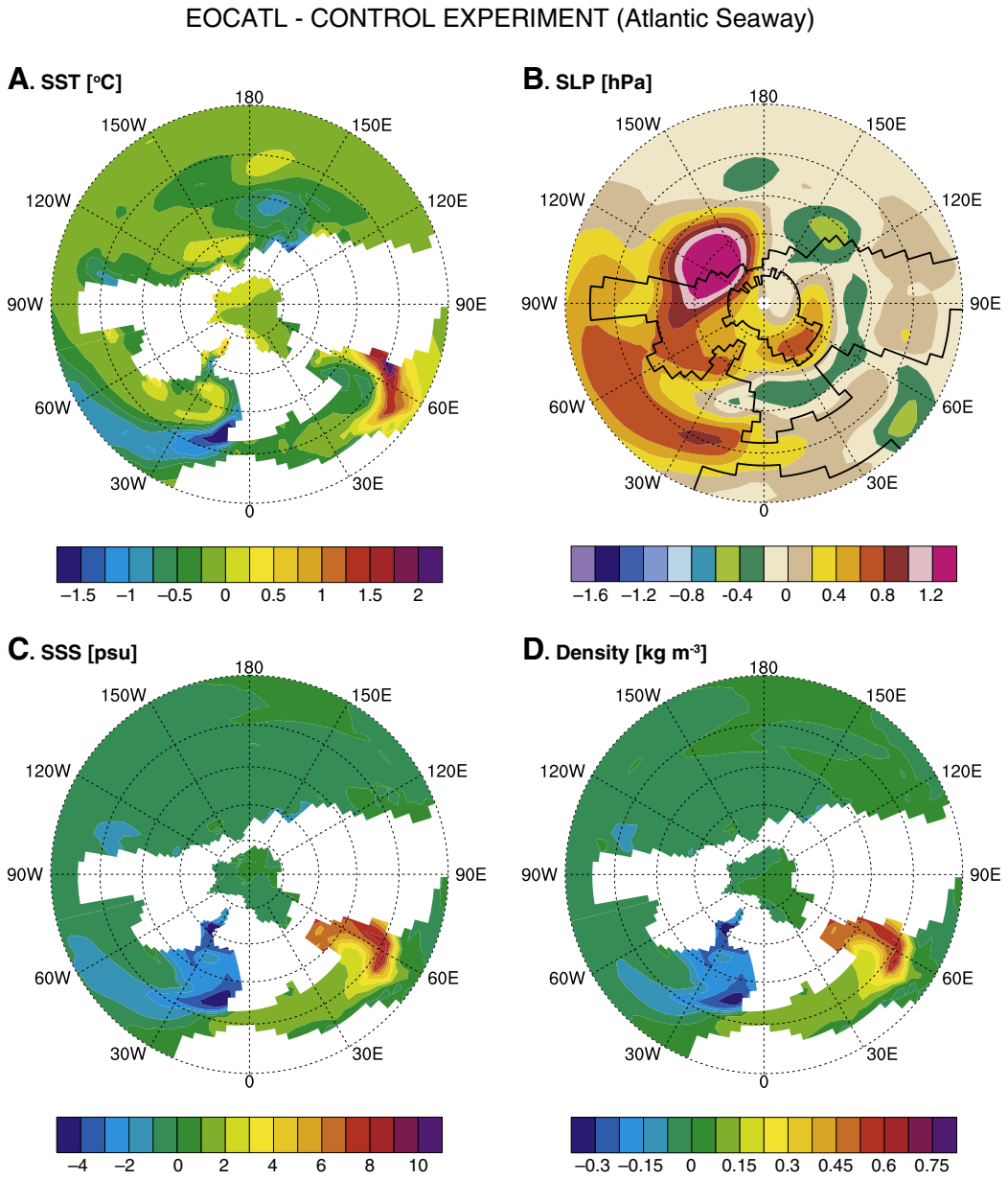

Fig. 6. Northern hemisphere polar projection from 15°N to 90°N, Control — EOCATL, annual average for years 1950–2000; A) sea surface temperature (°C), B) surface level pressure (hPa), C) surface salinity (psu), D) surface density.

Atlantic via an atmospheric teleconnection and associated changes in the buoyancy forcing.

4.1. Comparison of model simulations with climate proxies

Proxy temperature reconstructions for the Arctic (Brinkhuis et al., 2006; Eberle, 2006; Sluijs et al., 2006; Sluijs et al., 2009; Tripati et al., 2001; Weijers et al., 2007;) suggest temperatures of up to 23 °C during the PETM, whereas simulated model mean temperature are <10 °C. The highest Arctic surface ocean annual temperatures are produced in the Control and EOCATL experiments with average peak temperatures of ~10 °C. Although still significantly lower than proxy reconstructions, the change in Arctic surface temperatures associated with changes in fresh water flux to the global ocean supports the conclusions of Shellito et al. (2009) that changes in size or depth of Arctic passageways may have played a role in the high Arctic temperatures of the PETM. The Tripati and Elderfield (2005) reconstruction of deep-sea temperatures and circulation changes based upon $\delta^{18}O$ and $\delta^{13}C$ ratios, respectively, and Mg/Ca ratios from benthic foraminifera differ significantly from our model results. The foraminifera data suggests bottom water temperatures in the North Pacific (Shatsky Rise) and South Atlantic (Walvis Ridge) of around 17 °C. Changes in oxygen and carbon isotope levels are presented as evidence that convection and deep-water formation increased in the North Pacific and decreased in the Southern Ocean (Tripati and Elderfield, 2005). The Control and EOCATL experiments simulate temperatures around 9 °C throughout the deeper oceans; they also display the strongest deep-water formation in the North Pacific and Southern Ocean (Figs. 3 and 5). Changes in ocean temperatures at depths greater than 1000 m in the EOCATL and EOCPAC experiments are minimal, less than 1 °C (Fig. 4). The EOCPAC experiment reproduces little deep-water formation in the North Pacific, but does simulate stronger southward circulation at depths greater than ~1500 m, as well as a weak deep-water formation in the Southern Ocean. Overall, deep-water temperatures in the experiments are around 6 °C cooler than data presented in Tripati and Elderfield (2005). Increased temperature

with a decrease in deep-water formation in the North Pacific Ocean is in disagreement with the conclusion of Tripati and Elderfield (2005) that increased deep-water formation in the North Pacific would cause warming of intermediate waters. The EOCPAC experiment results of increased southward circulation in the North Pacific Ocean and deep-water formation in the North Atlantic Ocean, as well as reduced circulation in the Southern Ocean, do, however, support the modeling results of Bice and Marotzke (2002).

The discrepancy between the climate proxies from the sedimentary record and the Control experiment has been discussed in a previous study (Winguth et al., 2010). The high-latitude bias can be related to uncertainties in the reconstructions (diagenesis, dating, sampling size errors, and seasonal bias) and in the climate model (Zeebe et al., 2009), which include a model resolution not resolving seaways adequately, and sensitive model parameterizations, for example those associated with clouds (cloud albedo and cloud optical depth, or heat transport by tropical cyclones). The abundance of cloud condensation nuclei (CCN), which affects droplet formation and the albedo level of clouds (Kump and Pollard, 2008), as well as orbital parameters, affecting solar radiation distribution across the earth, might to be changed in order to resolve discrepancies between model and data. It is expected that the consideration of changes in the cloud optical depth would result in a further increase in ocean stratification and stagnation of the deep-sea circulation similar to the 16×CO_2 experiment in Winguth et al. (2010).

4.2. Circulation

The North Pacific source of deep water is substantially reduced by a freshwater influx from the Arctic in the North Pacific Ocean, leading to an increase in age of the water mass and nutrient concentrations in intermediate depths (~1200 m) in the EOCPAC experiment. The findings are agreeable with analysis of Nd isotope data suggesting that deep-water sources in the Pacific Ocean switched during the PETM from a bimodal ventilation of deep in the Northern and Southern Hemisphere to an intense ventilation from the Southern Ocean (Thomas et al., 2008).

Of the three sensitivity experiments, the EOCPAC experiment simulates the strongest $\delta^{13}C$ gradients from the northern Tethys and western Pacific Oceans into the Southern Ocean. An east-to-west flow in the equatorial Pacific is in agreement with circulation pattern inferred from $\delta^{13}C$ gradients (Nunes and Norris, 2006). At depths near 1200 m both the EOCATL and the EOCPAC experiment as well as in the control experiment show an average $\delta^{13}C$ gradient in the Atlantic Ocean of ~0.7 (Fig. 7), decreasing from north-to-south and in agreement with Nunes and Norris (2006). In all three experiments, a near stagnant southward directed flow of <2 Sv is simulated for the intermediate to deep North Atlantic Ocean. The source of intermediate water formation originate near the Gulf of Mexico (Winguth et al., 2010) flowing northward in the eastern basin at ~300 m depth and sinking into in the northern North Atlantic and sinking there in greater depth. These finding appear to be in contrast to strong northern North Atlantic source of deep water formation as proposed by Nunes and Norris (2006) from the interpretation of $\delta^{13}C$ gradients.

The open Fram Strait (EOCATL Experiment), as compared to a closed Fram Strait (Control experiment), produces a slightly enhanced southward overturning circulation at intermediate depth in response to increased surface stratification. While the open seaway scenario is generally in agreement with findings of Roberts et al. (2009), who used the GISS model, the closed seaway differs considerably. Water masses in CCSM-3 are highly stratified in the North Atlantic, whereas weakly stratified water masses in Roberts et al. (2009) produce a vigorous ventilation in the North Atlantic. Possible reasons for the contrasting results are differences in the surface buoyancy fluxes between the models (as shown in Fig. 6 compared to Fig. 6 in Roberts et al., 2009). The differences can be partially explained by lower CO_2 radiative forcing used in the scenario with a closed Fram Strait in the GISS model, leading to a lower precipitation, and higher North Atlantic surface salinity whereas in the 8×CO_2 Control experiment in CCSM-3 water masses in the North Atlantic are characterized by a higher static stability. Also, differences between GISS and CCSM-3 can be related to different model parameterizations and initializations (Randall et al., 2007) and a higher spatial and vertical resolution in CCSM-3.

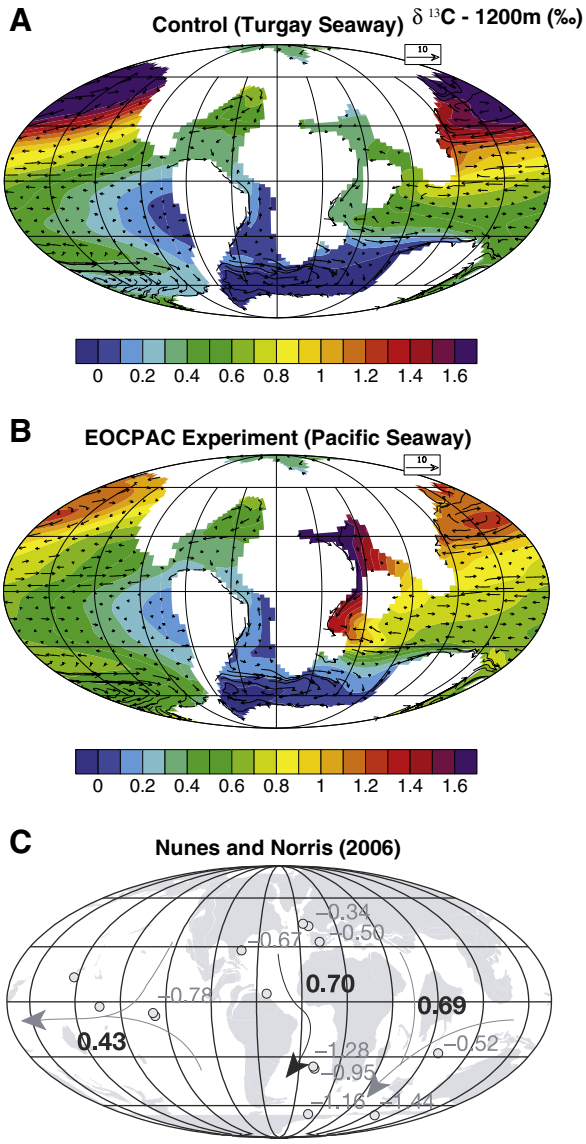

Fig. 7. Comparison of $\delta^{13}C$ gradients (‰) and horizontal velocities in (10–3 m), annual average years 1950–2000, between A) the Control experiment, B) EOCPAC experiment, and C) data from Nunes and Norris (2006).

4.3. Methane hydrate destabilization

Destabilization of methane hydrates in ocean sediments depends on multiple factors including an increase in temperature and/or a reduction of the critical pressure (Dickens et al., 1995, and Fig. 1 therein). Most hydrates are formed and are stable on the continental margins, specifically the slope and rise that are between 900 m and 2000 m (Dickens, 2001). A positive feedback loop responsible for the onset of the PETM due to the release of these hydrates is proposed in Bice and Marotzke (2002; see Fig. 9 therein). Initial increase in CO_2 in the atmosphere, caused possibly by volcanic outgassing, would

increase the strength of the hydrological cycle. These increases could cause a warming at intermediate depths within the ocean on a regional scale that could induce methane hydrate destabilization. This release of CH_4 would then oxidize to CO_2 in either the ocean or atmosphere and further exacerbate extremes in the hydrological cycle and eventually switch high southern latitude deep-water formation to high northern latitude deep-water formation.

The EOCPAC experiment illustrates a similar feedback loop (Fig. 8), though in response to an initial PETM warming rather than as a cause for it. Increased freshwater flux through the Bering Strait, for example by sea level rise, local tectonic changes, and/or thermal expansion, would decrease surface salinity and thereby surface density, reducing deep-water formation and deep overturning circulation from the North Pacific. Increased intermediate water circulation and advection of warm waters from the western and South Pacific could then serve to destabilize methane hydrates first in the North Pacific and then throughout the global ocean. The release of these hydrates and their subsequent oxidation to carbon dioxide entering both the ocean and atmosphere would further increase temperatures and serve to strengthen the PETM event.

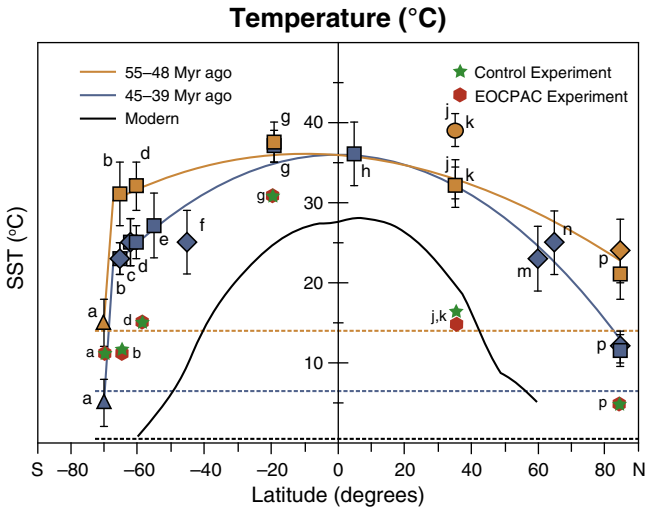

Fig. 9. Annual average of sea surface temperature (°C) for years 1950–2000 for Control and EOCPAC experiments in comparison with ODP data; figure after Bijl et al. (2009) and references therein.

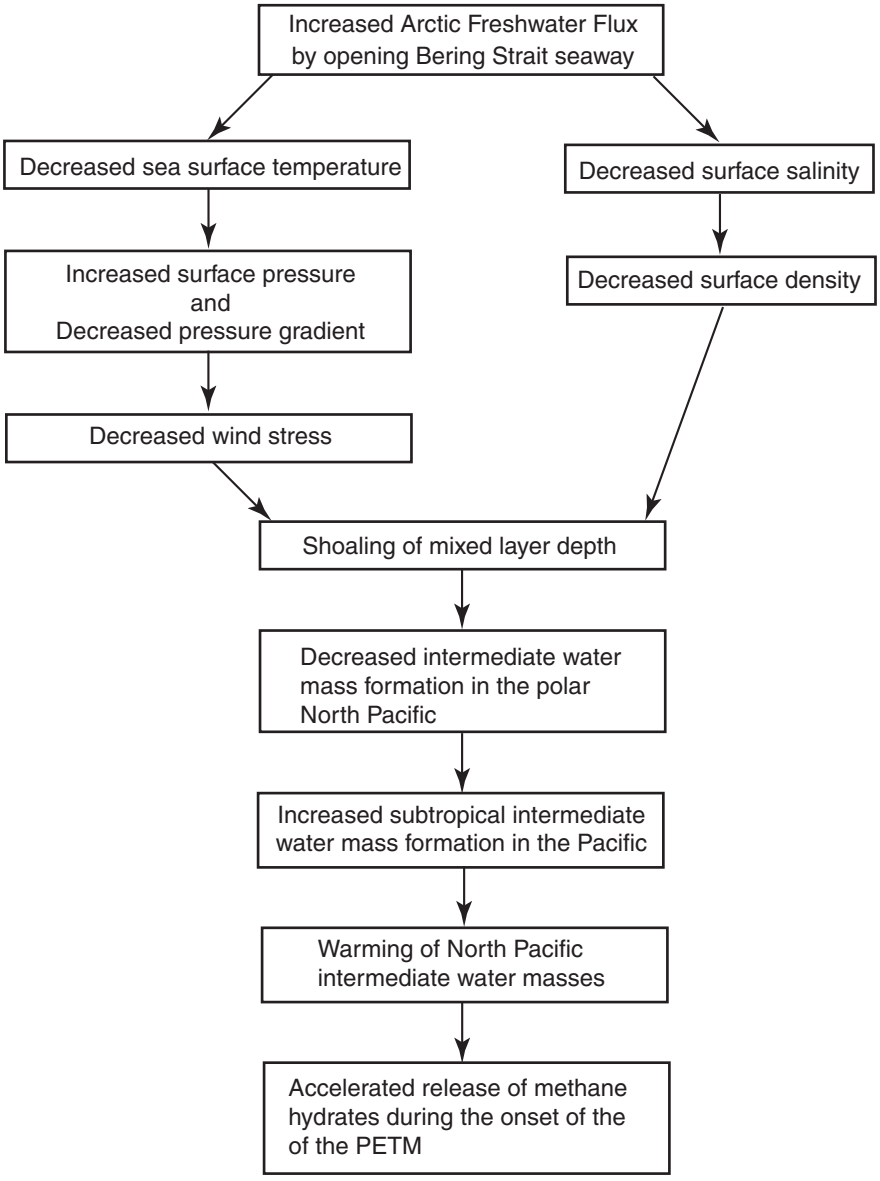

Fig. 8. Schematic showing the relationship between freshwater input from the Arctic and warming during the PETM.

Table 2
Surface, intermediate, and deep-water data-model temperature comparison (annual average years 1950–2000) for locations shown in Fig. 1. Paleolocations have been calculated using the PointTracker software by C. Scotese.

Name	Paleolocation	Data avg.	Age	Depth (m)	Data (°C)	Control avg. (°C)	Pacific avg. (°C)	Atlantic avg. (°C)
DSDP 277	60.6°S, 170.7°W	20.0	~51 Ma	Surface	20	11.7	11.6	11.6
Waipara River	52.1°S, 160.8°W	33.5	~51 Ma	Surface	30–37	14.3	14.1	14.3
Seymour Island	63.4°S, 64.1°W	12.0	~54–53 Ma	Surface	6–18	10.9	11.6	11.5
ODP 690	65.7°S, 7.2°W	18.5	PETM	Surface	17–20	11.9	11.9	11.8
DSDP 74	34.8°S, 10.5°W	N.A.	PETM	Surface	N.A.	23.7	23.5	23.4
Wilson Lake	39.7°N, 57.3°W	33.0	PETM	Surface	33	25.1	16.8	16.8
IODP 302	81.5°N, 42.6°E	23.0	PETM	Surface	23	3.2	2.4	2.8
ODP 865	8.3°N, 151.4°W	33.5	PETM	Surface	32–35	31.6	31.3	31.5
ODP 1209	23.6°N, 171.1°W	34.0	PETM	Surface	33–35	28.1	28	28
Tanzania	19.2°S, 30.9°E	32.0	PETM	Surface	30–34	30.9	30.9	30.8
Bighorn Basin	49.0°N, 89.5°W	23.0	PETM	Surface	20–26	9.5	9	9
Cerrejon Formation	8.4°N, 60.0°W	32.0	~58 Ma	Surface	30–34	31.2	30.3	30.1
DSDP 277	60.6°S, 170.7°W	15.0	~51 Ma	Seafloor	15	8.7	8.6	8.6
Waipara River	52.1°S, 160.8°W	21.5	~51 Ma	Intermediate	19–24	9.1–9.5	8.8–9.2	8.7–9.1
ODP 690	65.7°S, 7.2°W	16.0	PETM	~2100	14–18	9.3	9.1	9.1
DSDP 74	34.8°S, 10.5°W	14.5	PETM	~3100–3400	14–15	9.2	6.9	6.9
ODP 865	8.3°N, 151.4°W	15.0	PETM	~1300	13–17	10.4	10.7	10.3

5. Conclusions and summary

The experiments examined the effect that Arctic freshwater pulses would have on global ocean circulation, climate, and thereby the carbon cycle during the PETM. The experiments compared Arctic throughflow into the Pacific (EOCPAC) and Atlantic Oceans (EOCATL) against throughflow into the Indian/Tethys Ocean (Control).

Overall, both the EOCPAC and EOCATL experiments display noticeable changes in ocean properties relative to the Control experiment. All three experiments reproduce limited deep-water formation in the Southern Ocean in agreement with Thomas et al. (2008) but are not supportive of a strong source of deep water in the northern North Atlantic Ocean, in agreement with Panchuk et al. (2008) and Zeebe and Zachos (2007), and contrary to Nunes and Norris (2006). An increased southern circulation in the Pacific and Atlantic Oceans during the PETM in the EOCPAC experiment appears to agree well with previous modeling results from Bice and Marotzke (2002). The EOCPAC experiment, with a significantly reduced source of deep water in the North Pacific Ocean, matches the overturning circulation patterns of Nunes and Norris (2006) for the Pacific Ocean (see Fig. 3B therein).

From all three experiments the warmest deep-sea temperatures are simulated in the experiment with a seaway through the Bering Strait (EOCPAC). However, among the three experiments the Control experiment most closely simulates sea surface salinity (Pagani et al., 2006a) and temperature (Weijers et al., 2007) in the Arctic. It also reproduces the closest overall matches to global sea surface temperatures from the data (e.g. Bijl et al., 2009) (Fig. 9 and Table 2).

In conclusion, a flow through the Bering Strait produced a circulation pattern that could have contributed to triggering the release of methane hydrates by a remarkable warming of intermediate waters in the North Pacific. The increase in temperature in intermediate waters could have resulted in a dissociation of methane hydrates. The free methane would then have oxidized in the ocean or atmosphere increasing the carbon dioxide concentration in the atmosphere, hereby causing further warming of the atmosphere and ocean, and eventually accelerating methane hydrate destabilization on a global scale. The EOCPAC simulation indicates also, however, that freshwater input into the North Pacific would already cause a significant shift from northward overturning circulation at intermediate depths to southward overturning circulation and might in itself induce enough widespread warming of ocean waters to release CH_4 on a global scale. Physical and biogeochemical changes in the EOCPAC, EOCATL, and Control experiments, indicate not only that Arctic freshwater pulses may have played a significant role in the global climate and ocean circulation, and thus the carbon cycle during the PETM, but also that the location of Arctic seaways was an important factor.

A prediction of the lysocline depth in future studies would allow a more detailed comparison to data recovered from ODP sites, specifically the carbonate saturation profile produced by foraminifers and calcareous nannofossils (Kelly et al., 2005; Petrizzo, 2007; Zachos et al., 2005) and $[CO_3^{2-}]$ in the Atlantic and Pacific Oceans (Panchuk et al., 2008; Zeebe and Zachos, 2007). This capability within a fully coupled general circulation model would present an improvement in understanding of how a massive carbon release would affect the climate.

Acknowledgments

The graphics have been produced with support from Chandrika Nagaraj and Vinit Asher at UTA. We thank Christine Shield, Stephen Yeager, and Keith Lindsay at NCAR for stimulating discussions and technical support. The comments by Appy Sluijs and one anonymous reviewer greatly improved the quality of the manuscript. We are also grateful to Chris Scotese for his helpful comments as well as for using his PointTracker Software. All model simulations were done on NCAR computers, supported by NSF. The work is supported by NSF Grant EAR-0628394.

References

Antonov, J.I., Levitus, S., Boyer, T.P., 2005. Thermosteric sea level rise, 1955–2003. Geophysical Research Letters 32, L12602. doi:10.1029/2005GL023112.

Bice, K.L., Marotzke, J., 2002. Could changing ocean circulation have destabilized methane hydrate at the Paleocene/Eocene boundary? Paleoceanography 17, 1018. doi:10.1029/2001PA000678.

Bijl, P.K., Schouten, S., Sluijs, A., Reichart, G.-J., Zachos, J.C., Brinkhuis, H., 2009. Early Palaeogene temperature evolution of the Southwest Pacific Ocean. Nature 461, 776–779.

Bowen, G.J., Beerling, D.J., Koch, P.L., Zachos, J.C., Quattlebaum, T., 2004. A humid climate state during the Palaeocene/Eocene Thermal Maximum. Nature 432, 495–499.

Bowen, G.J., Bralower, T.J., Delaney, M.L., Dickens, G.R., Kelly, D.C., Koch, P.L., Kump, L.R., Meng, J., Sloan, L.C., Thomas, E., Wing, S.L., Zachos, J.C., 2006. Eocene hyperthermal event offers insight into greenhouse warming. Eos, Transactions, American Geophysical Union 87, 165–169.

Bralower, T.J., Premoli Silva, I., Malone, M.J., 2006. 1. Leg 198 Synthesis: a remarkable 120-m.y. record of climate and oceanography from Shatsky Rise, Northwest Pacific Ocean. In: Bralower, T.J., Premoli Silva, I., Molone, M.J. (Eds.), Proceedings of the Ocean Drilling Program, Scientific Results, Vol. 198, pp. 1–47.

Breecker, D.O., Sharp, Z.D., McFadden, L.D., 2010. Atmospheric CO_2 concentrations during ancient greenhouse climates were similar to those predicted for 2100 A.D. Proc. Natl. Acad. Sci. USA 107, 576–580.

Brinkhuis, H., Schouten, S., Collinson, M.C., Sluijs, A., Damsté, J.S.S., Dickens, G.R., Huber, M., Cronin, T.M., Onodera, J., Takahashi, K., Bujak, J.P., Stein, R., Burgh, J., Eldrett, J.S.,

Harding, I.C., Lotter, A.F., Sangiorgi, F., Cittert, H.K., Leeuw, J.W., Matthiessen, J., Backman, J., Moran, K., and the Expedition 302 Scientists, 2006. Episodic fresh surface waters in the Eocene Arctic Ocean. Nature 441, 606–609.
Broecker, W.S., Maier-Reimer, E., 1992. The influence of air and sea exchange on the carbon isotope distribution in the sea. Global Biogeochemical Cycles 6, 315–320.
Caldeira, K., Kasting, J.F., 1992. The life span of the biosphere revised. Nature 360, 721–723.
Clyde, W.C., Gingerich, P.D., 1998. Mammalian community response to the latest Paleocene Thermal Maximum: an isotaphonomic study in the Northern Bighorn Basin, Wyoming. Geology 26, 1011–1014.
Collins, W.D., Bitz, C.M., Blackmon, M.L., Bonan, G.B., Bretherton, C.S., Carton, J.A., Chang, P., Boney, S.C., Hack, J.J., Henderson, T.B., Diehl, J.T., Large, W.G., McKenna, D.S., Santer, B.D., Smith, R.D., 2006. The Community Climate System Model version 3 (CCSM3). Journal of Climate 19, 2122–2143.
Dickens, G.R., 2001. The potential volume of oceanic methane hydrates with variable external conditions. Organic Geochemistry 32, 1179–1193.
Dickens, G.R., 2004. Hydrocarbon-driven warming. Nature 429, 513–515.
Dickens, G.R., O'Neil, J.R., Rea, D.K., Owen, R.M., 1995. Dissociation of oceanic methane hydrate as a cause of the carbon isotope excursion at the end of the Paleocene. Paleoceanography 10, 965–971.
Doney, S.C., Lindsay, K., Fung, I., John, J., 2006. Natural variability in a Stable, 1000-Yr global coupled climate-carbon cycle simulation. Journal of Climate 19, 3033–3054.
Dorman, J.L., Sellers, P.J., 1989. A global climatology of Albedo, roughness length and stomatal resistance for atmospheric general circulation models as represented by the Simple Biosphere Model (SiB). Journal of Applied Meteorology 28, 833–855.
Eberle, J.J., 2006. Early Eocene Brontotheriidae (Perissodactyla) from the Eureka Sound Group, Ellesmere Island, Canadian high Arctic — implications for Brontothere origins and high-latitude dispersal. Journal of Vertebrate Paleontology 26, 381–386.
Gale, A.S., Hardenbol, J., Hathway, B., Kennedy, W.J., Young, J.R., Phansalkar, V., 2002. Global correlation of cenomanian (Upper Cretaceous) sequences: evidence for Milankovitch control on sea level. Geology 30, 291–294.
Gibbs, M.T., Rees, P.M., Kutzbach, J.E., Ziegler, A.M., Behling, P.J., Rowley, D.B., 2002. Simulation of permian climate and comparison with climate-sensitive sediments. Journal of Geophysical Research 93, 9341–9364.
Gibbs, J.S., Stoll, H.M., Bown, P.R., Bralower, T.J., 2010. Ocean acidification and surface water carbonate production across the Paleocene–Eocene Thermal Maximum. Earth and Planetary Science Letters 295, 583–592.
Gleason, J.D., Thomas, D.J., Moore Jr., T.C., Blum, J.D., Owen, R.M., Haley, B.A., 2009. Early to Middle Eocene history of the Arctic ocean from Nd–Sr Isotopes in fossil fish debris, Lomonosov Ridge. Paleoceanography 24, PA2215. doi:10.1029/2008PA001685.
Harding, I.C., Charles, A.J., Marshall, J.E.A., Pälike, H., Roberts, A.P., Wilson, P.A., Jarvis, E., Thorne, R., Morris, E., Moremon, R., Pearce, R.B., Akbari, S., 2011. Sea-level and salinity fluctuations during the Paleocene–Eocene Thermal Maximum in Arctic Spitsbergen. Earth and Planetary Science Letters 303, 97–107.
Heinemann, M., Jungclaus, J.H., Marotzke, J., 2009. Warm Paleocene/Eocene climate as simulated in ECHAM5/MPI-OM. Climate of the Past Discussions 5, 1297–1336.
Hollis, J.H., Handley, L., Crouch, E.M., Morgans, H.E.G., Baker, J.A., Creech, J., Collins, K.S., Gibbs, S.J., Huber, M., Schouten, S., Zachos, J.C., Pancost, R.D., 2009. Tropical sea temperatures in the high-latitude South Pacific during the Eocene. Geology 37, 99–102.
Hsieh, J.C.C., Yapp, C.J., 1999. Stable carbon isotope budget of CO_2 in a wet, modern soil as inferred from $Fe(CO_3)OH$ in Pedogenic Goethite: possible role of calcite dissolution. Geochimica et Cosmochimica Acta 63, 767–783.
Iakovleva, A.I., Heilmann-Clausen, C., 2007. Wilsonidium Pechoricum new species — a new dinoflagellate species with unusual asymmetry from the Paleocene/Eocene transition. Journal of Paleontology 81, 1020–1030.
Iakovleva, A.I., Brinkhuis, H., Cavagnetto, C., 2001. Late Palaeocene–Early Eocene dinoflagellate cysts from the Turgay Strait, Kazakhstan: correlations across ancient seaways. Palaeogeography, Palaeoclimatology, Palaeoecology 172, 243–268.
Ivany, L.C., Lohmann, K.C., Hasiuk, F., 2008. Eocene climate record of a high southern latitude continental shelf: Seymour Island, Antarctica. GSA Bull. 120, 659–678.
Kelly, D.C., Bralower, T.J., Zachos, J.C., 1998. Evolutionary consequences of the Latest Paleocene Thermal Maximum for tropical planktonic foraminifera. Palaeogeography, Palaeoclimatology, Palaeoecology 141, 139–161.
Kelly, D.C., Zachos, J.C., Bralower, T.J., Schellenberg, S.A., 2005. Enhanced terrestrial weathering/runoff and surface ocean carbonate production during the recovery stages of the Paleocene–Eocene thermal maximum. Paleoceanography 20, PA4023. doi:10.1029/2005PA001163.
Kennett, J.P., Stott, L.D., 1991. abrupt deep-sea warming, palaeoceanographic changes and Benthic extinctions at the end of the Palaeocene. Nature 353, 225–229.
Kump, L.R., Pollard, D., 2008. Amplification of Cretaceous warmth by biological cloud feedbacks. Science 320, 195.
Larson, K.M., Lowry, A.R., Kostoglodov, V., Hutton, W., Sánchez, O., Hadnut, K., Suárez, G., 2004. Crustal deformation measurements in Guerrero, México. Journal of Geophysical Research 109, B04409. doi:10.1029/2003JB002843.
Long, A.J., Shennan, I., 1994. Sea-level changes in Washington and Oregon and the "Earthquake Deformation Cycle". Journal of Coastal Research 10, 825–838.
Lunt, D.J., Valdes, P.J., Jones, T.D., Ridgwell, A., Haywood, A.M., Schmidt, D.N., Marsh, R., Maslin, M., 2010. CO_2-driven ocean circulation changes as an amplifier of Paleocene–Eocene thermal maximum hydrate destabilization. Geology 38, 875–878. doi:10.1130/G31184.1.
Maclennan, J., Jones, S.M., 2006. Regional uplift, gas hydrate dissociation and the origins of the Paleocene–Eocene Thermal Maximum. Earth and Planetary Science Letters 245, 65–80.
Maier-Reimer, E., 1993. Geochemical cycles in an ocean general circulation model: preindustrial tracer distributions. Global Biogeochem. Cycles 7, 645–677.
Markwick, P.J., 1997. Fossil crocodilians as indicators of Late Cretaceous and Cenozoic climates: implications for using paleontological data in reconstructing paleoclimate. Paleogeography 137, 205–271.
Meulenkamp, J.E., Sissingh, W., Beniamovskii, V.N., 2000. Map 17. Early/Middle Ypresian. In: Dercourt, J., Gaetani, M., Vrielynck, B., Barrier, E., Biju-Duval, B., Brunet, M.F., Cadet, J.P., Crasquin, S., Sandulescu, M. (Eds.), Atlas Peri-Tethys, Palaeogeographic Maps. Comission de la Carte Géologique du Monde, Paris.
Miller, K.G., Mountain, G.S., Browning, J.V., Kominz, M., Sugarman, P.J., Christie-Blick, M., Katz, M.E., Wright, J.D., 1998. Cenozoic global sea level, sequences, and the New Jersey transect: results from coastal plain and continental slope drilling. Reviews of Geophysics 36, 569–601.
Miller, K.G., Kominz, M.A., Browning, J.V., Wright, J.D., Mountain, G.S., Katz, M.E., Sugarman, P.J., Cramer, B.S., Christie-Blick, N., Pekar, S.G., 2005. The Phanerozoic record of global sea-level. Science 310, 1293–1298.
Najjar, R. G., Orr, J. C., 1999.Ocean Carbon-cycle Model Intercomparison Project OCMIP-2 Biotic HOWTO.unpublished manuscript. http://www.ipsl.jussieu.fr/OCMIP/.
Nunes, F., Norris, R.D., 2006. Abrupt reversal in ocean overturning during the Palaeocene/Eocene warm period. Nature 439, 60–63.
Pagani, M., Caldeira, K., Archer, D., Zachos, J.C., 2006a. An ancient carbon mystery. Science 314, 1556–1557.
Pagani, M., Pedentchouk, N., Huber, M., Sluijs, A., Schouten, S., Brinkhuis, H., SinninghеDamsté, J.S., Dickens, G.R., Expedition 302 Scientists, 2006b. Arctic hydrology during global warming at the Palaeocene/Eocene Thermal Maximum. Nature 442. doi:10.1038/nature05043.
Panchuk, K., Ridgwell, A., Kump, L.R., 2008. Sedimentary response to Paleocene-Eocene Thermal Maximum carbon release: a model-data comparison. Geology 36, 315–318.
Pearson, P.N., Palmer, M.R., 2000. Atmospheric carbon dioxide concentrations over the past 60 million years. Nature 406, 695–699.
Pearson, P.N., van Dongen, B.E., Nicholas, C.J., Pancost, R.D., Schouten, S., Singano, J.M., Wade, B.S., 2007. Stable warm tropical climate through the Eocene Epoch. Geology 35, 211–214.
Petrizzo, M.R., 2007. The onset of the Paleocene–Eocene Thermal Maximum (PETM) at sites 1209 and 1210 (Shatsky Rise, Pacific Ocean) as recorded by planktonic foraminifera. Marine Micropaleontology 63, 187–200.
Randall, D.A., Wood, R.A., Bony, S., Colman, R., Fichefet, T., Fyfe, J., Kattsov, V., Pitman, A., Shukla, J., Srinivasan, J., Stouffer, R.J., Sumi, A., Taylor, K.E., 2007. Cilmate models and their evaluation. In: Solomon, S., Qin, D., Manning, M., Chen, Z., Marquis, M., Averyt, K.B., Tignor, M., Miller, H.L. (Eds.), Climate Change 2007: The Physical Science Basis. : Contribution of Working Group I to the Fourth Assessment Report of the Intergovernmental Panel on Climate Change. Cambridge University Press, Cambridge, United Kingdom.
Roberts, C.D., LeGrande, A.N., Tripati, A.K., 2009. Climate sensitivity to arctic seaway restriction during the Early Paleogene. Earth and Planetary Science Letters 286, 576–585.
Schmitz, B., Pujalte, V., 2003. Sea-level, humidity, and land-erosion records across the initial Eocene thermal maximum from a continental-marine transect in northern Spain. Geology 31, 689–692.
Scotese, C.R., 2008. PALEOMAP project. www.scotese.com.
Sewall, J.O., Sloan, L.C., Huber, M., Wing, S., 2000. Climate sensitivity to changes in land surface characteristics. Global and Planetary Change 26, 445–465.
Shackleton, N.J., Kennett, J.P., 1975. Paleotemperature history of the Cenozoic and the initiation of Antarctic glaciation: oxygen and carbon isotope analyses in DSDP Sites 277, 279, and 281. In: Kennett, J.P., Houtz, M.R.E. (Eds.), Initial Reports of the Deep Sea Drilling Project, Vol. 29, pp. 743–755.
Shellito, C.J., Sloan, L.C., 2006. Reconstructing a lost Eocene paradise, part II: on the utility of dynamic global vegetation models in pre-quaternary climate studies. Global and Planetary Change 50, 18–32.
Shellito, C.J., Sloan, L.C., Huber, M., 2003. Climate model sensitivity to atmospheric CO2 levels in the Early-Middle Paleogene. Palaeogeography, Palaeoclimatology, Palaeoecology 193, 113–123.
Shellito, C.J., Lamarquie, J.-F., Sloan, L.C., 2009. Early Eocene Arctic climate sensitivity to pCO2 and basin geography. Geophysical Research Letters 36, L09707. doi:10.1029/2009GL037248.
Sluijs, A., Schouten, S., Pagani, M., Woltering, M., Brinkhuis, H., Damsté, J.S.S., Dickens, G.R., Huber, M., Reichart, G., Stein, R., Matthiessen, J., Lourens, L.J., Pedentchouk, N., Backman, J., Moran, K., the Expedition 302 Scientists, 2006. Subtropical Arctic Ocean temperatures during the Palaeocene/Eocene Thermal Maximum. Nature 441, 610–613.
Sluijs, A., Brinkhuis, H., Schouten, S., Bohaty, S.M., John, C.M., Zachos, J.C., Reichart, G., Damsté, J.S.S., Crouch, E.M., Dickens, G.R., 2007a. Environmental precursors to rapid light carbon injection at the Palaeocene/Eocene boundary. Nature 450, 1218–1221.
Sluijs, A., Bowen, G.J., Brinkhuis, H., Lourens, L.J., Thomas, E., 2007b. The Palaeocene–Eocene Thermal Maximum super greenhouse: biotic and geochemical signatures, age models and mechanisms of global change. In: Williams, M., Haywood, A.M., Gregory, F.J., Schmidt, D.N. (Eds.), Deep-Time Perspective on Climate Change: Marrying the Signal from Computer Models and Biological Proxies. : The Micropaleontological Society, Special Publications. The Geological Society, London, pp. 323–349.
Sluijs, A., Röhl, U., Schouten, S., Brumsack, H.-J., Sangiorgi, F., SinninghеDamsté, J.S., Brinkhuis, H., 2008. Arctic Late Paleocene–Early Eocene paleoenvironments with special emphasis on the Paleocene–Eocene Thermal Maximum (Lomonosov Ridge, Integrated Ocean Drilling Program Expedition 302). Paleoceanography 23, PA1S11. doi:10.1029/2007PA001495.
Sluijs, A., Schouten, S., Donders, T.H., Schoon, P.L., Röhl, U., Reichart, G.-J., Sangiorgi, F., Kim, J.-H., SinninghеDamsté, J.S., Brinkhuis, H., 2009. Warm and wet conditions in the Arctic region during Eocene Thermal Maximum 2. Nature Geoscience 2, 777–780.
Smith, R.D., Gent, P.R., 2004. Reference Manual for the Parallel Ocean Program (POP), Ocean Component of the Community Climate System Model (CCSM2.0 and 3.0).

Available online at Tech. Rep. LAUR-02-2484. Los Alamos National Laboratoryhttp://www.ccsm.ucar.edu/models/ccsm3.0/pop.
Speijer, R.P., Morsi, A.M., 2002. Ostracode turnover and sea-level changes associated with the Paleocene–Eocene thermal maximum. Geology 30, 23–26.
Storey, M., Duncan, R.A., Swisher III, C.C., 2007. Paleocene-Eocene Thermal Maximum and the opening of the Northeast Atlantic. Science 316, 587–589.
Svensen, H., Planke, S., Malthe-Sorenssen, A., Jamtvelt, B., Myklebust, R., Eidem, T.R., Rey, S.S., 2004. Release of methane from a volcanic basin as a mechanism for initial Eocene global warming. Nature 429, 542–545.
Thomas, E., 1998. The biogeography of the late Paleocene benthic foraminiferal extinction. In: Aubry, M.-P., Lucas, S., Berggren, W.A. (Eds.), Late Paleocene–early Eocene Biotic and Climatic Events in the Marine and Terrestrial Records. Columbia University Press, pp. 214–243.
Thomas, E., Shackleton, N.J., 1996. The Paleocene–Eocene benthic foraminiferal extinction and stable isotope anomalies. Geological Society, London, Special Publications 101, 401–441.
Thomas, D.J., Bralower, T.J., Zachos, J.C., 1999. New evidence for subtropical warming during the late Paleocene thermal maximum: stable isotopes from deep sea drilling project site 527, Walvis Ridge. Paleoceanography 14, 561–570.
Thomas, D.J., Zachos, J.C., Bralower, T.J., Thomas, E., Bohaty, S., 2002. Warming the fuel for the fire: evidence for the thermal dissociation of methane hydrate during the Paleocene–Eocene Thermal Maximum. Geology 30, 1067–1070.
Thomas, D.J., Bralower, T.J., Jones, C.E., 2003. Neodymium isotopic reconstruction of Late Paleocene–Early Eocene thermohaline circulation. Earth and Planeteary Science Letters 209, 309–322.
Thomas, D., Lyle, M., Moore Jr., T.C., Rea, D.K., 2008. Paleogene deep-water mass composition of the tropical Pacific and implications for thermohaline circulation in a greenhouse world. Geochemistry, Geophysics, Geosystems 9, 1–13. doi:10.1029/2007GC001748.
Tripati, A., Elderfield, H., 2005. Deep-sea temperature and circulation changes at the Paleocene–Eocene Thermal Maximum. Science 308, 1894–1898.
Tripati, A., Zachos, J., Marincovich Jr., L., Bice, K., 2001. Late Paleocene Arctic coastal climate inferred from molluscan stable and radiogenic isotope ratios. Palaeogeography, Palaeoclimatology, Palaeoecology 170, 101–113.
Waddell, L.M., Moore, T.C., 2008. Salinity of the Eocene Arctic Ocean from oxygen isotope analysis of fish bone carbonate. Paleoceanography 23, PA1S12. doi:10.1029/2007PA001451.
Wallace, J.M., Hobbs, P.V., 2006. Atmospheric Science: An Introductory Survey, second ed. Academic Press Publications, California.
Wanninkhof, R., 1992. Relationship between wind speed and gas exchange over the ocean. Journal of Geophysical Research 97, 7373–7382.
Watts, A.B., Thorne, J., 1984. Tectonics, global changes in sea level and their relationship to stratigraphical sequences at the US Atlantic continental margin. Marine and Petroleum Geology 1, 319–339.
Weijers, J.W.H., Schouten, S., Sluijs, A., Brinkhuis, H., Damsté, J.S.S., 2007. Warm arctic continents during the Palaeocene–Eocene Thermal Maximum. Earth and Planetary Science Letters 261, 230–238.
Wing, S.L., Harrington, G.J., Smith, F.A., Bloch, J.I., Boyer, D.M., Freeman, K.H., 2005. Transient floral change and rapid global warming at the Paleocene–Eocene Boundary. Science 310, 993–996.
Winguth, A.M.E., Heinze, C., Kutzbach, J.E., Maier-Reimer, E., Mikolajewicz, U., Rowley, D., Rees, A., Ziegler, A.M., 2002. Simulated warm polar currents during the middle Permian. Paleoceanography 17. doi:10.1029/2001PA000646.
Winguth, A.M.E., Shellito, C., Shields, C., Winguth, C., 2010. Climate response at the Paleocene–Eocene Thermal Maximum to greenhouse gas forcing — a model study with CCSM3. Journal of Climate 23, 2562–2584.
Woodburne, M.O., Gunnell, G.F., Stucky, R.K., 2009. Climate directly influences Eocene mammal faunal dynamics in North America. Proceedings of the National Academy of Sciences of the United States of America 106, 13399–13403.
Zachos, J.C., Pagani, M., Sloan, L., Thomas, E., Billups, K., 2001. Trends, rhythms, and aberrations in global climate 65 Ma to present. Science 292, 686–693.
Zachos, J.C., Wara, M.W., Bohaty, S., Delaney, M.L., Petrizzo, M.R., Brill, A., Bralower, T.J., Premoli-Silva, I., 2003. A transient rise in tropical sea surface temperature during the Paleocene–Eocene Thermal Maximum. Science 302, 1551–1554.
Zachos, J.C., et al., 2004. Proceedings of the Ocean Drilling Program, Initial Reports, Vol. 208. doi:10.2973/odp.proc.ir.208.2004. College Station, TX.
Zachos, J.C., Röhl, U., Schellenberg, S.A., Sluijs, A., Hodell, D.A., Kelly, D.C., Thomas, E., Nicolo, M., Raffi, I., Lourens, L.J., McCarren, H., Kroon, D., 2005. Rapid acidification of the ocean during the Paleocene–Eocene Thermal Maximum. Science 308, 1611–1615.
Zachos, J.C., Schouten, S., Bohaty, S., Quattlebaum, T., Sluijs, A., Brinkhuis, H., Gibbs, S.J., Bralower, T.J., 2006. Extreme warming of mid-latitude coastal ocean during the Paleocene–Eocene Thermal Maximum: inferences from TEX_{86} and isotope data. Geology 34, 737–740.
Zachos, J.C., Dickens, G.R., Zeebe, R.E., 2008. An Early Cenozoic perspective on greenhouse warming and carbon-cycle dynamics. Nature 451, 279–283.
Zeebe, R.E., Zachos, J.C., 2007. Reversed deep-sea carbonate ion basin gradient during Paleocene–Eocene Thermal Maximum. Paleoceanography 22, PA3201. doi:10.1029/2006PA001395.
Zeebe, R.E., Zachos, J.C., Dickens, G.R., 2009. Carbon dioxide forcing alone insufficient to explain Palaeocene–Eocene Thermal Maximum warming. Nature Geoscience 2, 576–580.